

## Article

# Experiment on the Properties of Soda Residue-Activated Ground Granulated Blast Furnace Slag Mortars with Different Activators

Yonghui Lin <sup>1,2,\*</sup> , Dongqiang Xu <sup>1</sup>, Wenguang Ji <sup>2</sup> and Xianhui Zhao <sup>3</sup>

<sup>1</sup> School of Civil and Transportation Engineering, Hebei University of Technology, Tianjin 300401, China; 2002021@hebut.edu.cn

<sup>2</sup> Department of Economics and Management, Hebei Normal University for Nationalities, Chengde 067000, China; zhxyjwg@163.com

<sup>3</sup> School of Civil Engineering, Hebei University of Engineering, Handan 056038, China; zhaoxianhui@hebeu.edu.cn

\* Correspondence: 201611601012@stu.hebut.edu.cn; Tel.: +86-187-1593-8682

**Abstract:** Soda residue (SR), a solid waste generated in the production of Na<sub>2</sub>CO<sub>3</sub> during the ammonia soda process, with a high pH value of 12, can be used as an activator of alkali-activated ground granulated blast furnace slag (GGBFS) cementitious materials. Three groups of experiments on SR-activated GGBFS mortars were designed in this paper to assess the role of the dominant parameters on fluidity and compressive strength of mortars. The results indicate that for fluidity and mechanical properties, the optimal scheme of SR-activated GGBFS mortars is 16:84–24:76 S/G, 0.01 NaOH/b, 0.05 CaO/b, and 0.50 w/b, with fluidity and compressive strength (28 d) of the mortars being 181–195 mm and 32.3–35.4 MPa, respectively. Between 2.5–10% CaCl<sub>2</sub> addition to CaO (5%)-SR (24%)-activated GGBFS mortar is beneficial to the improvement of the compressive strength of C<sub>2</sub>, whereas the addition of CaSO<sub>4</sub> is harmful. The main hydration products of mortars are ettringite, Friedel's salt, and CSH gels. The results provide a theoretical basis and data support for the utilization of SR.

**Keywords:** soda residue; ground granulated blast furnace slag; activator; mortar; orthogonal experiment; mechanical strength; hydration products; microstructure



**Citation:** Lin, Y.; Xu, D.; Ji, W.; Zhao, X. Experiment on the Properties of Soda Residue-Activated Ground Granulated Blast Furnace Slag Mortars with Different Activators. *Materials* **2022**, *15*, 3578. <https://doi.org/10.3390/ma15103578>

Academic Editor:  
Lenka Scheinherrová

Received: 1 May 2022  
Accepted: 16 May 2022  
Published: 17 May 2022

**Publisher's Note:** MDPI stays neutral with regard to jurisdictional claims in published maps and institutional affiliations.



**Copyright:** © 2022 by the authors. Licensee MDPI, Basel, Switzerland. This article is an open access article distributed under the terms and conditions of the Creative Commons Attribution (CC BY) license (<https://creativecommons.org/licenses/by/4.0/>).

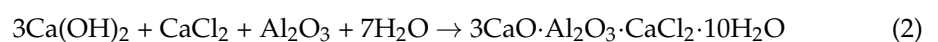
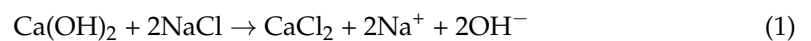
## 1. Introduction

Soda residue (SR) is an industrial solid waste of soda ash production by an ammonia-alkali process [1]. From 2017 to 2020, about 13 million tons of soda ash were produced annually through an ammonia-alkali process in China [2]. The production of 1 ton of soda ash generates about 0.3–0.6 tons of SR [3]. Thus, at least 3.9 million tons of SR are produced each year. However, only 5% of SR is recycled, mainly used to fill roadbeds [4]. Large amounts of untreated SR not only occupy land (In China, more than 15 km<sup>2</sup> of land was occupied), polluting the environment [4], but also lead to a waste of resources, so how to recycle it has become an urgent problem to be solved. Cement and alkali-activated slag cementitious materials (AAS) are one of the most widely used building materials at present. The cement-based cementitious materials made from SR could be an effective way to utilize SR in large quantities.

Ground granulated blast furnace slag (GGBFS) is a by-product material of pig iron [5,6]. Chemical components of GGBFS are mainly 27–40% SiO<sub>2</sub>, 30–50% CaO, 5–15% Al<sub>2</sub>O<sub>3</sub>, and 1–10% MgO [5]. GGBFS can be activated by alkaline materials (such as NaOH and CaO et al.) to generate AAS. Compared with Portland cement (PC), AAS can reduce carbon emissions [7], as traditional alkaline activators (NaOH, Na<sub>2</sub>SiO<sub>3</sub>) are expensive and have a great impact on the environment [8,9]. Ca(OH)<sub>2</sub> and CaO are potential alternatives to alkali activators because CaO (or Ca(OH)<sub>2</sub>)-activated slag cementitious materials can achieve

high 28 d compressive strength [10,11]. In addition, both  $\text{Ca}(\text{OH})_2$  and  $\text{CaO}$  are much less expensive than  $\text{NaOH}$  and  $\text{Na}_2\text{SiO}_3$ . The main mineral phases in SR are 39.6% calcite, 11.2% portlandite, 6%  $\text{NaCl}$ , 13.4  $\text{CaCl}_2$ , and 9.8%  $\text{CaSO}_4$  [12]. Owing to the existence of portlandite, SR has a high pH value, ranging from 11.8 to 12.0, with different mass ratios of SR to water (1:1–1:150) [13]. Pan [14] and Ma [15] reported that in AAS when the pore solution's pH value was greater than or equal to 10.5, Si and Al in slag were promoted to participate in the active reaction by destroying the glass chain on the surface of slag. Additionally, Song [16] considered that slag hydration reaction was activated or accelerated when the solution's pH value was higher than 11.5. Thus, in terms of the pH value of the solution, SR can provide a hydration environment for slag.

Previous studies [17–19] investigated the usage of SR instead of limestone as a cement raw material or a mineral additive to produce cement. However, this method is not widely used due to the high concentration of chloride ions in SR, which may lead to corrosion of steel. Compared with PC, AAS has a stronger ability to solidify chloride ions [20,21] because slag is rich in Al-phase, which can react with  $\text{NaCl}$  or  $\text{CaCl}_2$  to form Friedel's salt (Fs), as shown in Equations (1) and (2) [22,23]. Additionally, numerous studies [8,24–26] have demonstrated that SR can provide a hydration environment for AAS, and  $\text{Ca}^{2+}$ ,  $[\text{SO}_4]^{2-}$  and  $\text{Cl}^-$  ions contained in SR can also participate in the hydration reaction of slag, generating ettringite (AFt) and Fs. However, there is still a risk of steel corrosion due to the presence of  $\text{Cl}^-$  ions in SR, so it is a better choice to utilize SR in the unreinforced concrete field [27,28]. Xu [27] used 30% SR, 45% GGBFS, 15% steel slag, and 10% desulfurization gypsum to prepare clinker-free concrete, and the 28 d compressive strength of the concrete could reach up to 38.3 MPa. Song [26] prepared mortar using SR, GGBFS, and cement (mass ratio was 2:6:2), and the compressive strength could reach 45.1 MPa. Sun [29] took 30% SR, 23% GGBFS, and 30% fly ash as main raw materials, adding 12% gypsum and 5% alkaline activator ( $\text{Na}_2\text{SiO}_3$ ), and prepared cementitious materials, the compressive strength of which could reach 35.2 MPa at 28 d. Therefore, SR can be used as the raw material for the preparation of cementitious materials.



Different kinds and amounts of raw materials affect the compressive strength of cementing materials. According to tests and results of previous studies [12,13,30], the 8–24% mass ratio of SR replacing GGBFS gave high compressive strength (27.6–33.7 MPa) of the SR-activated GGBFS cementitious material at 28 d and low compressive strength (0.6–1.6 MPa) at early ages (3 d). Using SR and fly ash (mass ratio was 2:3) to prepare the geopolymer, Zhao [4] reached a similar conclusion.  $\text{NaOH}$  and  $\text{CaO}$  could activate GGBFS and dissolve its silicon and aluminum structure, generating hydration products [31]. In SR-activated GGBFS cementitious materials, the low content of  $\text{NaOH}$  ( $\text{NaOH}$  to GGBFS mass ratio was 1%) was beneficial to the improvement of compressive strength of the cementitious materials, while the high content of  $\text{NaOH}$  (5–10%) was not [30]. It might be because a low concentration of  $\text{NaOH}$  could provide a better hydration environment for slag. Relevant studies [32,33] show that pH value between 12.6 and 13.0 was the best environment for the hydration reaction of cement-based materials to produce hydration products. Additionally, the water-cement ratio also affected the compressive strength of cementitious materials [34,35]. It can be seen that the amount of SR, alkali activators ( $\text{NaOH}$ ,  $\text{CaO}$ ), and water-cement ratio all affect the compressive strength of SR-activated GGBFS cementitious materials.

The reason for strength enhancement derived from  $\text{CaO}$  for alkali-activated cementitious materials [36,37] is that  $\text{CaO}$  reacted with water to generate  $\text{Ca}(\text{OH})_2$ , which consumed water in the solution, further strengthened local alkalinity, and accelerated the release of silicon, aluminum, and calcium from raw material particles, thus facilitating the silica-aluminum polymerization reaction. Additionally, the heat released by  $\text{CaO}$  in

water increased the local temperature of the solution and promoted the polymerization of silicon and aluminum [38]. Zhang [39] considered that a small amount of gypsum could accelerate the hydration of alkali-activated slag pastes and was beneficial to the formation of the skeleton structure of mortar. However, an excessive amount of gypsum caused large amounts of ettringite generation, leading to stress concentration in mortar and strength reduction of mortar. Yum [36,40] found that  $\text{CaCl}_2$  could improve the compressive strength of the pastes at different ages, increase the cumulative reaction heat within 72 h, accelerate the dissolution of GGBFS, and increase the number of reaction products.

In this paper, the strength development of SR-activated GGBFS mortars with different admixtures was investigated in three groups of experiments in order to explore the factors influencing compressive strength. For Group I, an orthogonal experiment was used to determine the effects of SR to GGBFS mass ratio, NaOH to binder (SR and GGBFS mixture) mass ratio, CaO to binder mass ratio, and water to binder mass ratio on physical and the mechanical properties of the mortars. For Group II, the optimal mixing ratio of mortars was determined. For Group III, experiments were designed to clarify the effects of calcium compounds with different anionic species on mechanical properties of the mortars. Finally, the hardened cementitious materials were characterized by X-ray diffraction (XRD) and scanning electron microscopy (SEM). The obtained results would provide a guideline and reference for the use of SR in the field of AAS cementitious materials.

## 2. Materials and Methods

### 2.1. Materials

Raw materials of SR-activated GGBFS mortar are SR (provided by Tangshan Sanyou Chemical Industry Co., Ltd., Tangshan, China), GGBFS (provided by Tangshan Xinrong Slag Powder Co., Ltd., Tangshan, China), and ISO standard sand (Xiamen Iso Standard Sand Co., Ltd., Xiamen, China). NaOH, CaO,  $\text{CaCl}_2$ , and  $\text{CaSO}_4$  are selected as mortar admixtures. The chemical and physical properties of SR and GGBFS are referenced in the previous studies [12,13]. The BET surface area of SR and GGBFS are  $409 \text{ m}^2/\text{kg}$  and  $450 \text{ m}^2/\text{kg}$ , respectively. The pH value of SR and GGBFS are 12.0 and 10.7, respectively. The XRD patterns and the SEM images of the SR and the GGBFS are shown in Figure 1.

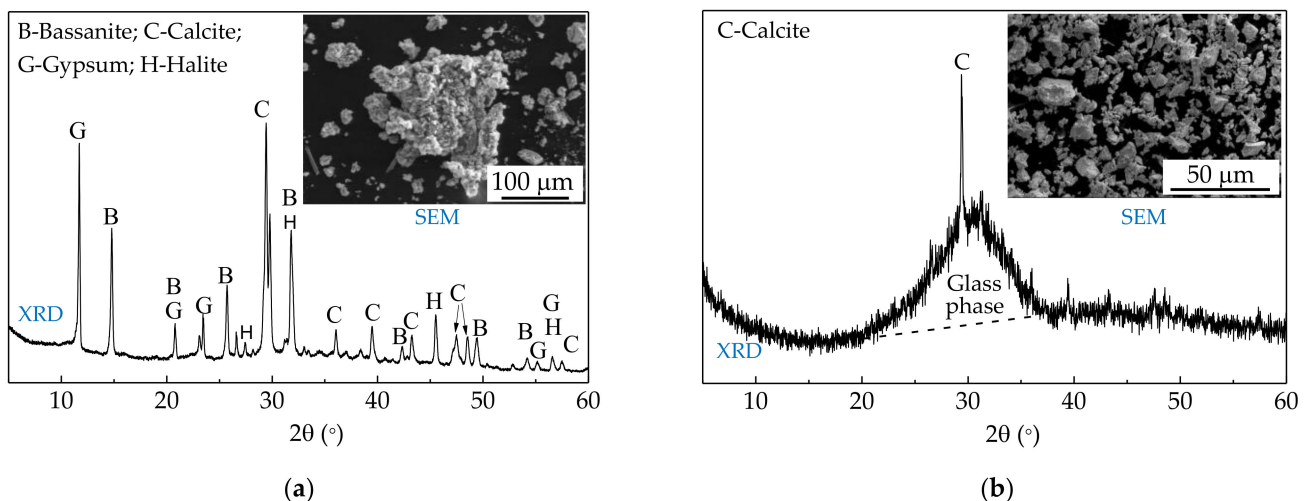


**Figure 1.** XRD patterns and SEM images: (a) SR; (b) GGBFS.

The main mineral phases in the SR are 39.6% calcite, 11.2% portlandite, 6% NaCl, 13.4%  $\text{CaCl}_2$ , and 9.8%  $\text{CaSO}_4$ . The GGBFS was mainly composed of 41.4% CaO, 28.1%  $\text{SiO}_2$ , 14.8%  $\text{Al}_2\text{O}_3$ , and 9.5% MgO. The specific gravity and fineness modulus of ISO standard sand are 2.6 and 2.9, respectively. All the admixtures are of analytical grade, as shown in Table 1.

**Table 1.** Purity of admixture.

Reagents	Purity (%)	Solubility	Production Place
NaOH	96.0	soluble	Tianjin, China
CaO	98.0	slightly soluble	Tianjin, China
CaCl <sub>2</sub>	96.0	soluble	Tianjin, China
CaSO <sub>4</sub>	97.0	slightly soluble	Tianjin, China

## 2.2. Preparation of Specimens

Based on previous study results [12,13,30] and analysis, three groups of experiments were designed in this paper. For group I, an orthogonal experiment (nine kinds of mortars) was employed to assess the role of the dominant parameters with 4 factors and 3 levels, as shown in Table 2.

**Table 2.** Group I, 4 factors and 3 levels selected for the experimental design.

Factor	Level 1	Level 2	Level 3
S/G	8:92	16:84	24:76
NaOH/b	0	0.005	0.01
CaO/b	0	0.025	0.05
w/b	0.46	0.50	0.54

The 4 factors and 3 levels are: (1) SR to GGBFS mass ratio (S/G): 8:92, 16:84, and 24:76; (2) NaOH to binder (SR and GGBFS mixture) mass ratio (NaOH/b): 0, 0.005, and 0.01; (3) CaO to binder mass ratio (CaO/b): 0, 0.025, and 0.05; (4) water to binder mass ratio (w/b): 0.46, 0.50, and 0.54. Details of mix proportions are given in Table 3.

**Table 3.** Group I, mixing proportions of mortars according to the experimental design in Table 2 (g).

No.	SR	GGBFS	NaOH	CaO	Water	Sand
M1	36	414	0	0	207	1350
M2	36	414	2.25	11.25	225	1350
M3	36	414	4.50	22.50	243	1350
M4	72	378	0	11.25	243	1350
M5	72	378	2.25	22.50	207	1350
M6	72	378	4.50	0	225	1350
M7	108	342	0	22.50	225	1350
M8	108	342	2.25	0	243	1350
M9	108	342	4.50	11.25	207	1350

For group II, based on the range analysis of the fluidity and the compressive strength (3 and 28 d) acquired by orthogonal experiment, mortars with optimal mixing ratios were selected and tested (Table 4).

**Table 4.** Group II, optimal experiment of mortars (g).

No.	SR	GGBFS	NaOH	CaO	Water	Sand
O1	72	378	4.50	22.50	225	1350
O2	108	342	4.50	22.50	225	1350
O3	108	342	4.50	11.25	243	1350

For group III, experiments were designed to analyze the influence of calcium compounds (CaO, CaSO<sub>4</sub>, and CaCl<sub>2</sub>) with different anionic species on mortar, in which water to solids (SR mixed with GGBFS, and one or more of CaO, CaSO<sub>4</sub>, and CaCl<sub>2</sub>) mass ratio is 0.5, as shown in Table 5.

**Table 5.** Group III, mixing proportions of SR-activated GGBFS mortars (g).

No.	SR	GGBFS	CaO	CaSO <sub>4</sub>	CaCl <sub>2</sub>	Water	Sand
C0	108	342	-	-	-	225.0	1350
C1	108	342	11.25	-	-	230.6	1350
C2	108	342	22.50	-	-	236.3	1350
C3	108	342	45.00	-	-	247.5	1350
CS1	108	342	22.50	11.25	-	241.9	1350
CS2	108	342	22.50	22.50	-	247.5	1350
CS3	108	342	22.50	45.00	-	258.8	1350
CC1	108	342	22.50	-	11.25	241.9	1350
CC2	108	342	22.50	-	22.50	247.5	1350
CC3	108	342	22.50	-	45.00	258.8	1350
CC4	108	342	22.50	-	67.50	270.0	1350
CSC1	108	342	22.50	11.25	11.25	247.5	1350
CSC2	108	342	22.50	11.25	22.50	253.1	1350
CSC3	108	342	22.50	22.50	22.50	258.8	1350
CSC4	108	342	22.50	11.25	45.00	264.4	1350

In preparation for the experiments, the raw SR was first crushed and dried in an oven at 105 °C for 12 h and then ground to a particle size less than 0.075 mm, with a BET surface area of 409 m<sup>2</sup>/kg, as described in the previous study [11]. According to GB/T 17671-1999 (ISO) standard (China) [38], SR, GGBFS, and admixture powders were firstly well mixed for 3 min, and then water was added and mixed for another 3 min. After that, the ISO standard sand was added and mixed for 3 min to prepare fresh homogenized mortars. The mortars were molded into 40 mm × 40 mm × 160 mm prismatic molds with two layers. Each layer was vibrated for 1 min to remove entrained air. The prepared mortars with molds were then placed in sealed plastic bags to avoid the loss of water and prevent carbonization and cured in a chamber at 25 ± 3 °C and 95 ± 5% RH (relative humidity). After 24 h curing, the mortars were demolded and further cured until testing.

### 2.3. Testing and Characterization

The fluidity of designed fresh mortars was measured by a fluidity tester (NLD-3, Cangzhou Jingruida Test Instrument Co. Ltd., Cangzhou, China) as illustrated in the literature [41] and the Chinese standard GB/T 2419-2005 [42]. According to the GB/T 17671-1999 (ISO) standard (China) [43] and the literature [12], the compressive and flexural strength of specimens were measured by a model YAW-300 machine (Shanghai Suns Machinery Manufacturing Co., Ltd., Shanghai, China) with 2400 and 50 N/s loading rate, respectively. The porosity of mortars was measured according to the ASTM C20-2000 (2005) standard [44] and the literature [13]. Fluidity, porosity, compressive strength, and flexural strength were measured and averaged from 3, 3, 6, and 3 specimens, respectively. The XRD patterns were recorded on a Rigaku D/Max-2500 X-ray diffractometer (Akishima, Tokyo, Japan) with CuK $\alpha$  radiation using a generator voltage of 40 kV and 150 mA, from 6° to 40° at 4°/min. The microstructure of mortars was tested by SEM (Quanta JEOL JSM-7610FPlus, Rigaku, Tokyo, Japan). SEM images were taken at 2 kV, 10,000 $\times$ .

## 3. Results and Discussion

### 3.1. Orthogonal Experiment

#### 3.1.1. Fluidity

The fluidity of freshly mixed mortar determines whether the mortar can be mixed, placed, consolidated, and finished. According to the GB 175-2007 standard (China) [45], the fluidity of fresh mortar should be no less than 180 mm. The fluidity of fresh mortars by orthogonal experiment is presented in Figure 2, where the fluidity of mortars varies greatly with different S/G, NaOH/b, CaO/b and w/b.

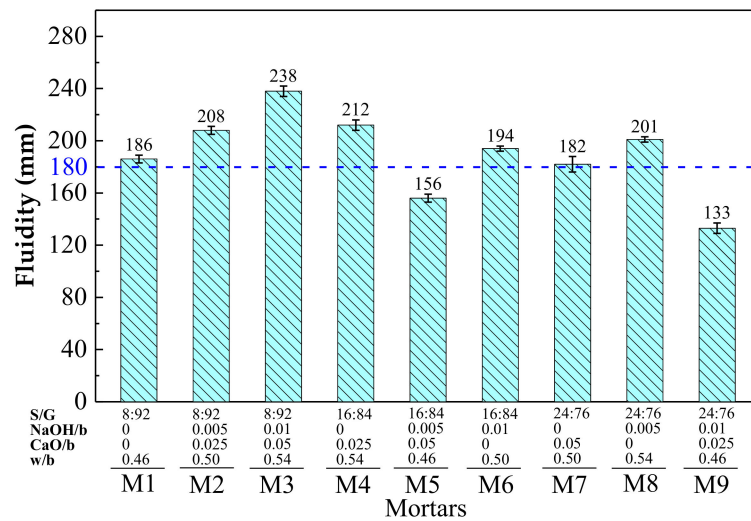


Figure 2. Fluidity of flesh mortars by orthogonal experiment.

The range analysis results of fluidity by orthogonal experiment are shown in Table 6. The ranking sequence of the factors influencing fluidity is  $w/b > S/G > CaO/b > NaOH/b$ . The range results ( $R_j$ ) of  $w/b$  and  $S/G$  are much higher than those of  $CaO/b$  and  $NaOH/b$ , indicating that  $w/b$  and  $S/G$  play a major role in the fluidity of mortar.

Table 6. Orthogonal extreme difference analysis of fluidity (mm).

Index	Factors				Rank
	S/G	NaOH/b	CaO/b	w/b	
$M_{1j}$	211	193	194	158	$w/b > S/G > CaO/b > NaOH/b$
$M_{2j}$	187	188	184	195	
$M_{3j}$	172	188	192	217	
$R_j$	39	5	9	59	
Trend	↘	↔	↘ ↗	↗	

Note:  $M_{ij}$  is average value of measured data of orthogonal experiment at  $i$  level and  $j$  column;  $R_j = M_{jmax} - M_{jmin}$ .  
 '↘', '↗', and '↔' represent the increasing trend, the decreasing trend, unchanged, respectively.

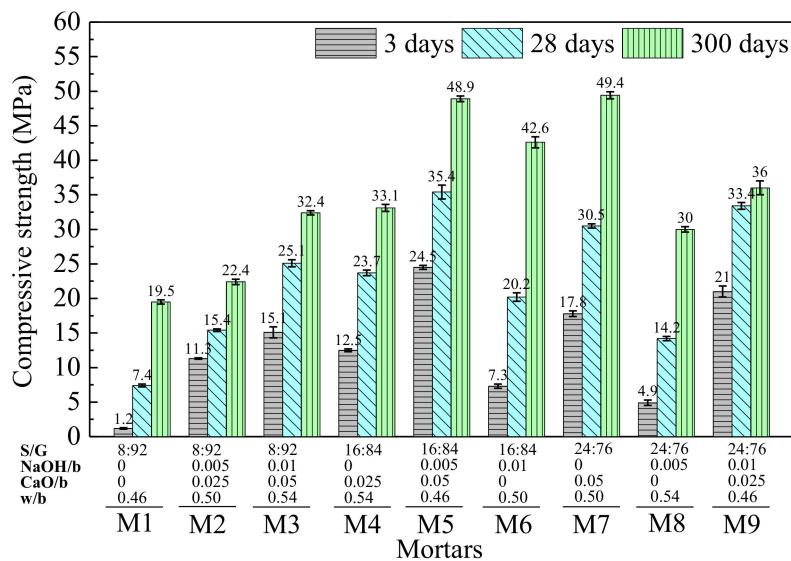
With the increase of  $w/b$ , the fluidity of mortar increases. It is because that with the increase of free water, SR and GGBFS particles are better dispersed in water, reducing the probability of physical agglutination in mortar. It is worth noting that the fluidity of most mortars meets the standard except that of M5 and M9, with a low  $w/b$  (0.46), as shown in Figure 2.

With the increase of  $S/G$ , the fluidity of mortar decreases. Study [24] found that the physical water absorption of SR was the key factor causing the decrease of mortar fluidity. With the increase of  $S/G$ , more free water is entrapped in the pores of SR, which is adverse to fluidity. Thus, when SR proportion is increased,  $w/b$  should also be increased to ensure good workability of mortar.

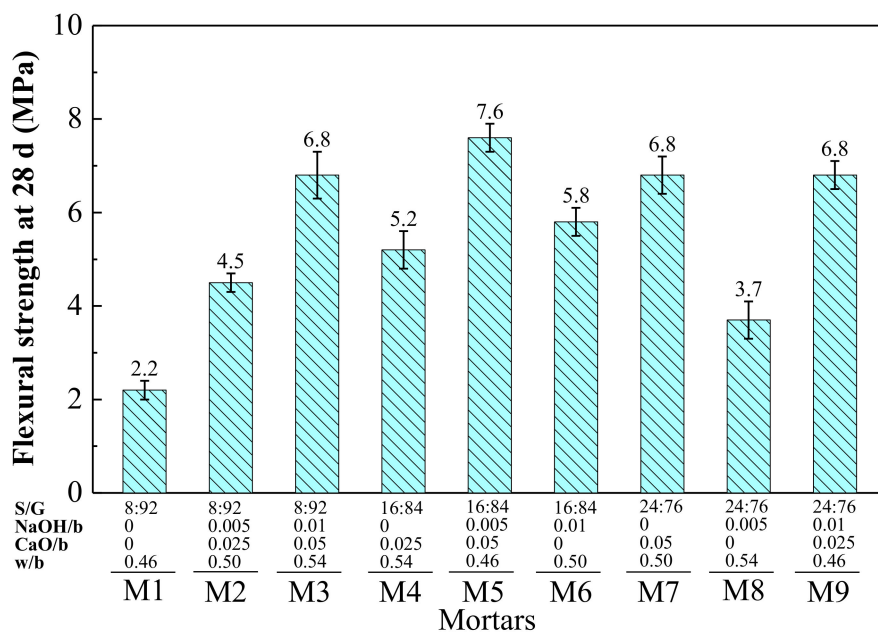
### 3.1.2. Mechanical Strength

The results of mechanical properties by orthogonal experiment (compressive strength at 3, 28, and 300 d, and flexural strength at 28 d) are shown in Figure 3. It can be found that the compressive strength of all mortars increases with the increase of curing age and is much higher at 300 d. Among all the mortars, M5 shows the highest compressive strength at 3 and 28 d (24.5 and 35.4 MPa) and flexural strength at 28 d (7.6 MPa); M7 shows the highest compressive strength at 300 d. When  $S/G$  is 8:92, the early compressive strength (3 d) of M2 (11.3 MPa) and M3 (15.1 MPa) is much higher than that of M1 (1.2 MPa).

It indicates that the increase of NaOH, CaO, and water improves the compressive strength of SR-activated GGBFS mortar.



(a)



(b)

Figure 3. Orthogonal experiment results of (a) compressive strength at 3, 28, and 300 d; (b) flexural strength at 28 d.

The range analysis results of mechanical properties by orthogonal experiment are shown in Table 7.

**Table 7.** Orthogonal extreme difference analysis of mechanical strength (MPa).

Index	Index	Factors				Rank
		S/G	NaOH/b	CaO/b	w/b	
3 d Compressive Strength	M <sub>1j</sub>	9.200	10.500	4.467	15.567	CaO/b > S/G > w/b > NaOH/b
	M <sub>2j</sub>	14.767	13.567	14.933	12.133	
	M <sub>3j</sub>	14.567	14.467	19.133	10.833	
	R <sub>j</sub>	5.567	3.967	14.666	4.734	
	Trend	↗ ↘	↗	↗	↘	
28 d Compressive Strength	M <sub>1j</sub>	15.967	20.533	13.933	25.400	CaO/b > S/G > NaOH/b > w/b
	M <sub>2j</sub>	26.433	21.667	24.167	22.033	
	M <sub>3j</sub>	26.033	26.233	30.333	21.000	
	R <sub>j</sub>	10.466	5.700	16.400	4.400	
	Trend	↗ ↘	↗	↗	↘	
300 d Compressive Strength	M <sub>1j</sub>	24.767	34.000	30.700	34.800	S/G > CaO/b > w/b > NaOH/b
	M <sub>2j</sub>	41.533	33.767	30.500	38.133	
	M <sub>3j</sub>	38.467	37.000	43.567	31.833	
	R <sub>j</sub>	16.766	3.233	13.067	6.300	
	Trend	↗ ↘	↘ ↗	↘ ↗	↗ ↘	
28 d Flexural Strength	M <sub>1j</sub>	4.500	4.733	3.900	5.533	CaO/b > NaOH/b > S/G > w/b
	M <sub>2j</sub>	6.200	5.267	5.500	5.700	
	M <sub>3j</sub>	5.767	6.467	7.067	5.233	
	R <sub>j</sub>	1.700	1.734	3.167	0.467	
	Trend	↗ ↘	↗	↗	↗ ↘	

Ranking sequences of factors influencing compressive strength of the mortars at 3, 28, and 300 d are CaO/b > S/G > w/b > NaOH/b, CaO/b > S/G > NaOH/b > w/b, and S/G > CaO/b > w/b > NaOH/b, respectively. It can be seen that S/G and CaO/b have a greater influence on compressive strength during the whole curing time, whereas w/b and NaOH/b have a lesser influence. With the increase of CaO/b, compressive strength at 3, 28, and 300 d increases and reaches its maximum value when CaO/b is 0.05. With the increase of S/G, compressive strength (3, 28 and 300 d) increases first and then decreases. When S/G is 16:84, compressive strength reaches its maximum value. The mean values of levels 2 and 3 at 3, 28, and 300 days were 14.767 MPa and 14.567 MPa, 26.433 MPa and 26.033 MPa, 41.533 MPa and 38.467 MPa, respectively. It can be found that the differences in mean values between levels 2 and 3 in each age were almost negligible. Therefore, it can be concluded that when S/G is in the range of 16:84–24:76, the mortars activated by SR can obtain higher compressive strength. With the increase of w/b, compressive strength at 3 d and 28 d decreases, while compressive strength at 300 d increases first and then decreases and reaches its maximum value when w/b is 0.50. Considering the long-term compressive strength and workability of fresh mortars, the optimal value of w/b is 0.50. NaOH/b has little effect on compressive strength, and the maximum value of compressive strength is reached when NaOH/b is 0.01 at each age. Therefore, for compressive strength, the optimal scheme is 16:84–24:76 S/G, 0.01 NaOH/b, 0.05 CaO/b, and 0.50 w/b.

The ranking sequence of factors influencing flexural strength of the mortars at 28 d is CaO/b > NaOH/b > S/G > w/b. CaO/b and NaOH/b have a greater effect on flexural strength at 28 d, and the optimal value of CaO/b is 0.05 and 0.01. When S/G is 16:84, flexural strength reaches its maximum value. When S/G is 24:76, a slight strength decrease was found. Flexural strength at 28 d reaches its maximum value when w/b is 0.50. Therefore, for flexural strength, the optimal scheme is 16:84–24:76 S/G, 0.01 NaOH/b, 0.05 CaO/b, and 0.50 w/b at 28 d.

In conclusion, for mechanical properties, the optimal scheme is 16:84–24:76 S/G, 0.01 NaOH/b, 0.05 CaO/b, and 0.50 w/b.

### 3.2. Optimized Experiment of Mortars

According to the test results and the analysis in Section 3.1, it can be known that when S/G is 16:84 or 24:76, NaOH/b is 0.01, CaO/b is 0.05, and w/b is 0.50, the mortars can obtain high compressive strength. Thus, the optimal mortars, O1 (S/G, NaOH/b, CaO/b, and w/b are 16:84, 0.01, 0.05, and 0.50, respectively), O2(S/G, NaOH/b, CaO/b, and w/b are 24:76, 0.01, 0.05, and 0.50, respectively) are chosen to do further tests. Compared with O1, the SR in O2 is increased, which will lead to a decrease in the fluidity of the mortar. In order to increase the amount of solid waste SR in the mortar and ensure the fluidity of the mortar, it is necessary to design another optimal mortar, O3 (S/G, NaOH/b, CaO/b, and w/b are 24:76, 0.01, 0.05, and 0.54, respectively). The detailed test scheme is shown in Table 4, and the performance index of the mortars is shown in Table 8.

**Table 8.** Performance index of mortars.

No.	Fluidity (mm)	Porosity (%)	Compressive Strength (MPa)		28 d Flexural Strength (MPa)
			3 d	28 d	
O1	191 ± 4	20.5 ± 0.5	22.9 ± 0.6	32.3 ± 0.4	8.0 ± 0.2
O2	181 ± 3	21.2 ± 0.4	24.3 ± 1.1	35.4 ± 0.9	7.1 ± 0.3
O3	195 ± 4	22.7 ± 0.6	21.9 ± 0.8	33.0 ± 0.7	7.1 ± 0.4
M7	182 ± 6	21.9 ± 0.5	17.8 ± 0.4	30.5 ± 0.3	6.8 ± 0.4

It can be seen that the fluidity of the three optimal mortars (O1, O2, and O3) is larger than 180 mm, which meets the requirements of the standard [45]. Compared with O1, the compressive strength of O2 is higher, indicating that under the synergistic effect of NaOH and CaO, the increase of SR is beneficial to the improvement of compressive strength. It may be because SR has strong water absorption, and the increase of SR decreases the w/b of mortar. According to the orthogonal experiment, the decrease of w/b is conducive to the improvement of compressive strength. Similarly, the reason why the compressive strength of O3 decreases, compared with O2, is the increase of w/b. The increase of SR is not conducive to the improvement of flexural strength, which is because SR, with abundant pore structure, increases the porosity of mortar. Therefore, when S/G, NaOH/b, CaO/b, and w/b are 16:84–24:76, 0.01, 0.05, and 0.50, respectively, the fluidity and the compressive strength at 28 d are 181–195 mm and 32.3–35.4 MPa, respectively.

Compared with O2, M7 in an orthogonal experiment has similar values in fluidity and porosity. Additionally, though M7 also has a higher compressive strength at 28 d, it is 4.9 MPa lower than O2. M7 is likely to be more popular with the engineering community because it does not use NaOH in its raw materials, reducing the cost of mortar and the potential for alkali toxicity. Thus, the compressive strength of M7 can be improved by admixtures, which will be further explained in Section 3.3.

### 3.3. Effects of Anionic Calcium Compounds on Compressive Strength

The orthogonal experiment results and the analysis show that CaO is beneficial to the improvement of the compressive strength of SR-activated GGBFS mortars. When CaO (5%) is added into SR (24%)-activated GGBFS (76%) mortar, the compressive strength of mortar (M7) can reach 30.5 MPa at 28 d. In order to further study the effect of different anionic calcium compounds (CaO, CaSO<sub>4</sub>, CaCl<sub>2</sub>) on the mechanical properties of SR-activated GGBFS mortars, experimental schemes were designed, as shown in Table 5. The compressive strength (28 d) of SR-activated GGBFS mortars with different activators is shown in Figure 4.

#### 3.3.1. Influence of CaO on Compressive Strength

The compressive strength of SR (24%)-activated GGBFS (76%) mortar (C0) at 3 d and 28 d is 3.7 and 23.1 MPa, respectively. The compressive strength of C0 at the early age (3 d) is very low. The addition of CaO (2.5–10%) can improve the compressive strength of mortar, especially at an early age. When the CaO proportion is 5%, the compressive strength of

mortar (C2) reaches its maximum at 3 d and 28 d, 15.0 MPa and 29.6 MPa, respectively, which are about 4 times and 1.3 times higher than those of C0. Relevant studies [36,37] show that CaO can accelerate the hydration of GGBFS. CaO reacts with water to generate  $\text{Ca}(\text{OH})_2$ , which consumes water in the solution, further enhances local alkalinity, and accelerates the release of calcium, aluminum, and silicon phases from GGBFS particles, resulting in the generation of hydration products, such as CSH and CAH gel. It is worth noting that when the proportion of CaO is 10%, the compressive strength of mortar (C3) is improved compared with that without CaO (C0). However, compared with C2, where the CaO proportion is 5%, the compressive strength of C3 at 3 and 28 d is significantly reduced. It may be because excessive CaO cannot fully disperse in mortar, resulting in the agglomeration of CaO, which becomes the weak link of mortar, and leads to the decline of compressive strength [46].

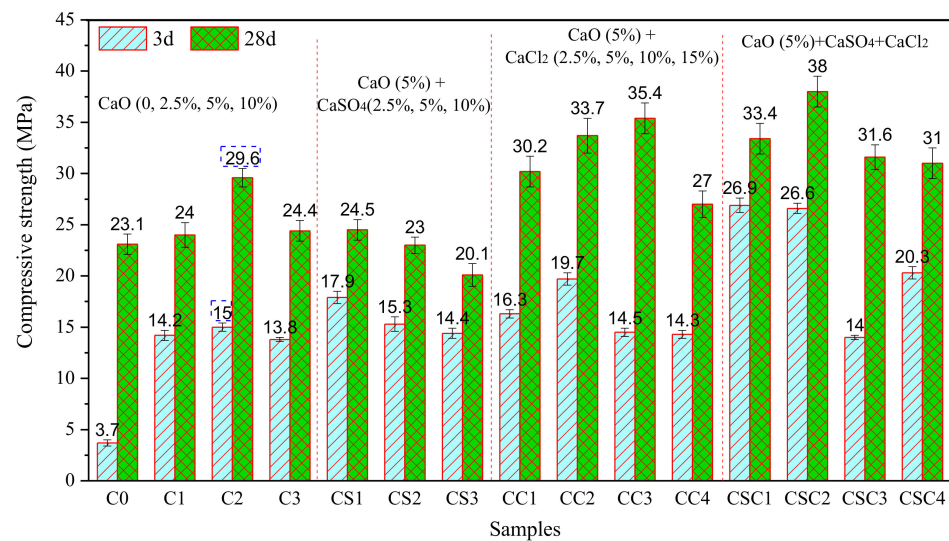


**Figure 4.** Compressive strength of SR-activated GGBFS mortars with different activators.

### 3.3.2. Influence of $\text{CaSO}_4$ on Compressive Strength

On the basis of C2, the effect of  $\text{CaCl}_2$  on the compressive strength of CaO-SR-activated GGBFS mortars (CC1, CC2, CC3, CC4) was discussed by adding  $\text{CaCl}_2$  (2.5%, 5%, 10%, and 15%, respectively). It can be seen that a low proportion of  $\text{CaSO}_4$  (2.5–5%) is beneficial to the improvement of compressive strength of mortar at early age, whereas a 10% addition of  $\text{CaSO}_4$  decreases the compressive strength at an early age. The compressive strength of mortars (CS1, CS2, and CS3) with  $\text{CaSO}_4$  (2.5%, 5%, and 10%) at 28 d is lower than that of C2. It may be because with the increasing addition of  $\text{CaSO}_4$ ,  $[\text{SO}_4]^{2-}$  in mortars increases. Under the alkaline environment,  $\text{Ca}^{2+}$  and  $[\text{AlO}_4]^{5-}$  are released from GGBFS rapidly and react with  $[\text{SO}_4]^{2-}$  to produce a large amount of ettringite (Equation (3)), which inserts into the pores of mortar and serves as a powerful skeleton structure, and improves early compressive strength. However, in the progress of the reaction, a large amount of ettringite is attached to the surface of SR and GGBFS. Further hydration of GGBFS is prevented, resulting in weaker compressive strength at 28 d. Additionally, Zhang [39] believes that when  $\text{CaSO}_4$  in alkali-activated GGBFS exceeds 2%, a large amount of ettringite will generate. The expansion of ettringite will lead to the concentration of stress in mortar, and the decrease of volume stability, thus reducing the compressive strength of mortar. According to the mineral composition of SR in Section 2.1 and the proportion of SR in C2, by calculation, C2 contains 2.35%  $\text{CaSO}_4$ , which exceeds the requirement of  $\text{CaSO}_4$  addition (2%) in a previous study [39]. It can be seen that when SR addition is 24%, extra addition of  $\text{CaSO}_4$  is harmful to the development of the compressive strength of mortar.



### 3.3.3. Influence of CaCl<sub>2</sub> on Compressive Strength

On the basis of C2, the effect of CaCl<sub>2</sub> on the compressive strength of CaO-SR-activated GGBFS mortars (CC1, CC2, CC3, CC4) was discussed by adding CaCl<sub>2</sub> (2.5%, 5%, 10%, and 15%, respectively). It can be seen that 2.5–5% addition of CaCl<sub>2</sub> is beneficial to the improvement of the early compressive strength of the CaO-SR-activated GGBFS mortar. It is because CaCl<sub>2</sub> can accelerate the generation of CSH gel and Fs, which is conducive to compressive strength [20]. When the proportion of CaCl<sub>2</sub> exceeds 5%, the early compressive strength decreases, which may be because excessive CaCl<sub>2</sub> leads to the existence of a large amount of Ca<sup>2+</sup> ions in the solution. Under the common ion effect [47], the pH value of the solution reduces, and calcium, aluminum, and silicon phases dissolved from the GGBFS are not enough to generate CSH and Fs. The compressive strength of the CaO-SR-activated GGBFS mortar at 28 d increases first and then decreases with the addition of CaCl<sub>2</sub> from 2.5% to 15%, and reaches its maximum value of 35.4 MPa when the addition of CaCl<sub>2</sub> is 10%. When CaCl<sub>2</sub> addition is 15%, the 28 d compressive strength is only 27 MPa, lower than that of C2 (29.6 MPa). Therefore, a 2.5–10% CaCl<sub>2</sub> addition is beneficial to the improvement of compressive strength.

### 3.3.4. Influence of CaSO<sub>4</sub> and CaCl<sub>2</sub> on Compressive Strength

On the basis of C2, an experiment was carried out to study the influence of composite activator, including CaSO<sub>4</sub> and CaCl<sub>2</sub>, on compressive strength of mortars (CSC1, with 2.5% CaSO<sub>4</sub> and 2.5% CaCl<sub>2</sub>; CSC2, with 2.5% CaSO<sub>4</sub> and 5% CaCl<sub>2</sub>; CSC3, with 5% CaSO<sub>4</sub> and 5% CaCl<sub>2</sub>; CSC4, with 2.5% CaSO<sub>4</sub> and 10% CaCl<sub>2</sub>). When the addition of CaSO<sub>4</sub> is 2.5%, the compressive strength of the mortars increases first and then decreases with the addition of CaCl<sub>2</sub>, rising from 2.5% to 10%. When CaCl<sub>2</sub> addition is 5% (CSC2), the maximum value of compressive strength at 28 d is 38.0 MPa. Compared with CSC2, CaSO<sub>4</sub> in CSC3 increases to 5%, and the compressive strength of the mortar at each age (3 d and 28 d) decreases significantly. It can be seen that a low proportion of CaSO<sub>4</sub> and CaCl<sub>2</sub> are conducive to the compressive strength of CaO-SR-activated GGBFS mortars.

## 3.4. Hydration Products

### 3.4.1. XRD Analysis

The XRD patterns of C0, C1, C2, C3, CS1, CC2, CC3, and CSC3 at 28 d are shown in Figure 5. It can be seen from Figure 5a that the main mineral phases in C0 (SR (24%)-activated GGBFS mortar) are bassanite, calcium chloride, CSH gel, ettringite, Fs, portlandite and quartz. CSH gel, ettringite, Fs, and portlandite are hydration products of C0, which is consistent with the previous research [13]. The mineral phases, bassanite and calcium chloride come from SR, and quartz comes from ISO standard sand. Compared with C0, the XRD pattern of C1 shows a new characteristic reflection of ettringite ( $2\theta = 9.249^\circ$ ,  $d = 0.96$  nm), indicating that 2.5% CaO addition accelerates the hydration of GGBFS, and more Ca<sup>2+</sup> and [AlO<sub>4</sub>]<sup>5-</sup> released from GGBFS react with [SO<sub>4</sub>]<sup>2-</sup> to produce ettringite. In terms of compressive strength, C1 is stronger than C0. In XRD patterns of C2 and C3, the characteristic reflections of bassanite disappear, indicating that the bassanite in SR is completely consumed to generate ettringite.

Compared with C2, in the XRD pattern of CS1, with 2.5% CaSO<sub>4</sub> addition, the characteristic reflections of bassanite ( $2\theta = 14.739^\circ$ ,  $d = 0.06$  nm;  $2\theta = 31.811^\circ$ ,  $d = 0.28$  nm) appear, indicating that CaSO<sub>4</sub> in mortar is excessive. Compared with C2, in the XRD patterns of CC2 and CC3, with 5% and 10% CaCl<sub>2</sub> addition, fewer ettringite reflections are found. It may be due to more Ca<sup>2+</sup> and [AlO<sub>4</sub>]<sup>5-</sup> being released from GGBFS, and ettringite converts into Fs in the presence of high concentrations of CaCl<sub>2</sub> [48], as shown in Equations (4) and (5) [47,49]. However, when CaSO<sub>4</sub> and CaCl<sub>2</sub> with equal mass are added, both ettringite and Fs exist in the hydration of CSC3. It can be seen that a high concentration of CaCl<sub>2</sub> can reduce the amount of ettringite in mortar.



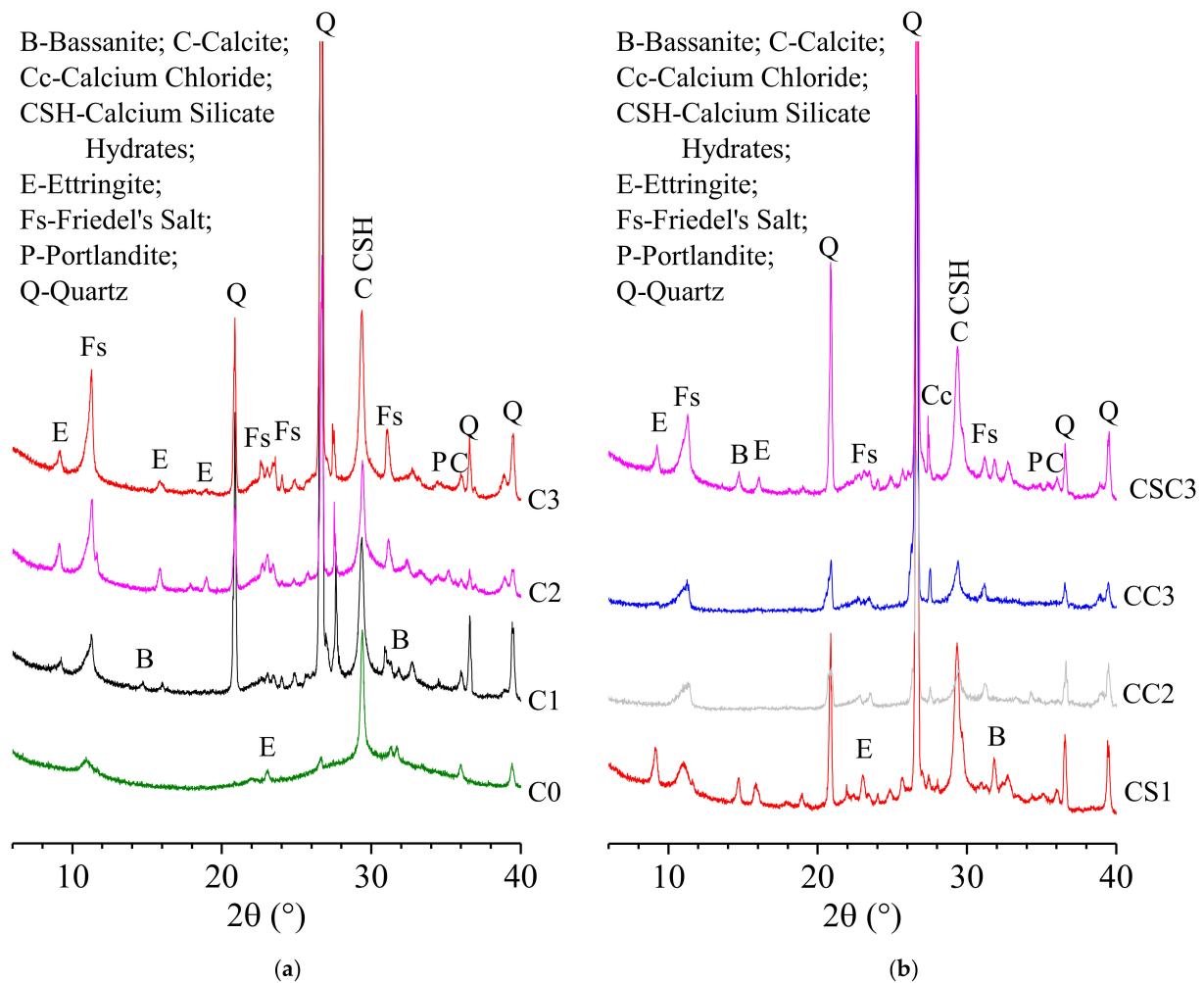
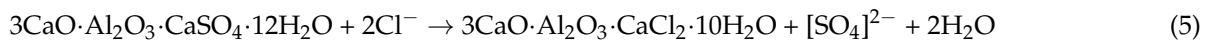


**Figure 5.** XRD patterns of (a) C0, C1, C2, and C3 at 28 d; (b) CS1, CC2, CC3, and CSC3 at 28 d.

### 3.4.2. SEM Analysis

Figure 6 shows SEM images of mortars (C0, C1, C2, C3, CS1, CC2, and CSC3) with different activators at 28 d. The microstructure of C0 (Figure 6a) has a large amount of needle-like ettringite (AFt), flat hexagonal Fs, and honeycomb-like CSH gels, filling the pores or adhering to the particles of SR, GGBFS, and sand. However, a large number of pores still exist, and the microstructure of C0 is not dense. With the increase of the addition of CaO from 2.5% to 10%, AFt, Fs, and CSH gels increase and fill the pores among the particles of mortars (C1–C3, Figure 6b–d). Additionally, AFt and Fs are covered with the CSH gels. The addition of 2.5% CaSO<sub>4</sub> to mortar (Figure 6e) can also improve the hydration of GGBFS and generate more AFt and CSH gels. With the addition of 5% CaCl<sub>2</sub> to mortar (Figure 6f), more Fs and CSH gels generate, but less AFt. In CSC3 (Figure 6g), under the influence of CaSO<sub>4</sub> and CaCl<sub>2</sub>, the microstructure of the mortar is denser, macroscopically exhibiting higher compressive strength (38.0 MPa) at 28 d, which is in consistency with the results described in Section 3.3.4.

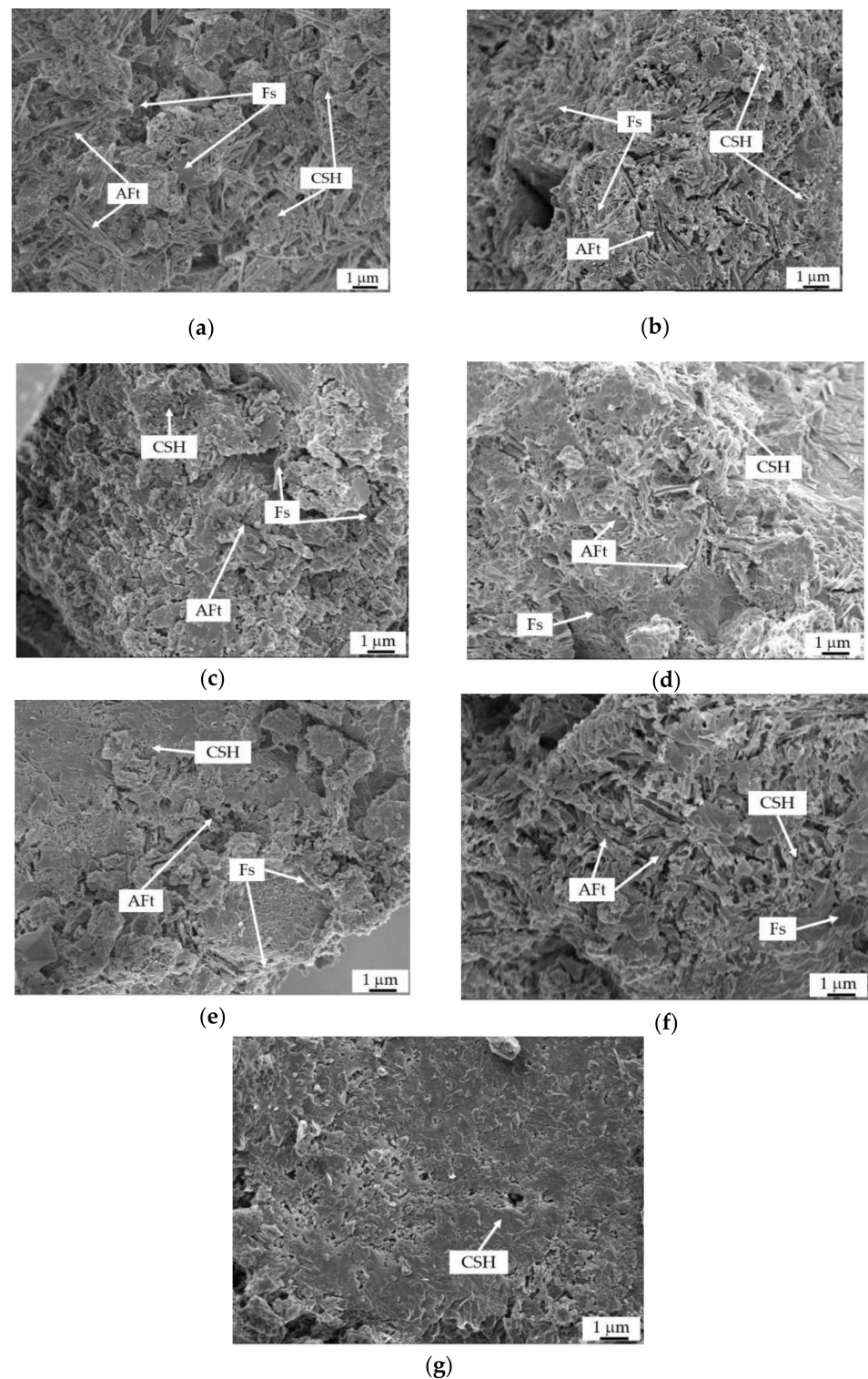


**Figure 6.** SEM images of mortars at 28 d: (a) C0; (b) C1; (c) C2; (d) C3; (e) CS1; (f) CC2; (g) CSC3.

#### 4. Conclusions

In this study, three groups of experiments are designed, including an orthogonal experiment with 4 factors and 3 levels, an optimized experiment, and an experiment on SR-activated GGBFS mortars with different anionic calcium compounds activators. Fluidity, mechanical strength, porosity, hydration products, and microstructure of mortars were studied. Based on the obtained results, the following conclusions are made.

1. The ranking sequences of factors influencing compressive strength of the mortars at 3, 28, and 300 d are  $\text{CaO/b} > \text{S/G} > \text{w/b} > \text{NaOH/b}$ ,  $\text{CaO/b} > \text{S/G} > \text{NaOH/b} > \text{w/b}$ , and  $\text{S/G} > \text{CaO/b} > \text{w/b} > \text{NaOH/b}$ , respectively;
2. S/G and CaO/b have a greater influence on compressive strength during the whole curing time. When CaO/b is 0.05 and S/G is 16:84–24:76, the mortars activated by SR can obtain high compressive strength;
3. For mechanical properties and fluidity, the optimal scheme of SR-activated GGBFS mortars is 16:84–24:76 S/G, 0.01 NaOH/b, 0.05 CaO/b, and 0.50 w/b. Compressive strength at 28 d and fluidity of the mortars are 32.3–35.4 MPa, and 181–195 mm, respectively;
4. Compressive strength of CaO (5%)-SR (24%)-activated GGBFS mortars (C2) at 3 d and 28 d can reach 15.0 MPa and 29.6 MPa, respectively. Between 2.5–10%  $\text{CaCl}_2$  addition is beneficial to the improvement of compressive strength, whereas  $\text{CaSO}_4$  is harmful;
5. The main hydration products of mortars are AFt, Fs, and CSH gels. High concentration of  $\text{CaCl}_2$  can reduce the amount of ettringite in mortars.

**Author Contributions:** Conceptualization, Y.L. and D.X.; methodology, Y.L., W.J. and X.Z.; validation, Y.L. and D.X.; formal analysis, Y.L. and W.J.; investigation, Y.L.; resources, D.X.; data curation, Y.L.; writing—original draft preparation, Y.L. and X.Z.; writing—review and editing, Y.L. and W.J.; visualization, Y.L.; supervision, D.X.; project administration, D.X.; funding acquisition, Y.L. and D.X. All authors have read and agreed to the published version of the manuscript.

**Funding:** This research was funded by the Science and Technology Project Foundation of Hebei Province, China (grant number 16273809), the P.H.D Innovation Project Foundation of Hebei University of Engineering, China (grant number SJ2101003126), and the Tianjin Research Innovation Project for Postgraduate Students (grant number 2021KJ078).

**Institutional Review Board Statement:** Not applicable.

**Informed Consent Statement:** Not applicable.

**Data Availability Statement:** Not applicable.

**Conflicts of Interest:** The authors declare no conflict of interest.

## References

1. Wang, Z.; Lyu, X. Preparation of Ca–Si–Al–Mg Porous Ceramics by Co-Operation of Ca&Mg-Contained Soda Residue and Altered Rock Gold Tailings. *J. Clean. Prod.* **2020**, *262*, 121345.
2. National Bureau of Statistics of China. Available online: <http://www.stats.gov.cn/tjsj/ndsj/> (accessed on 17 April 2022).
3. Li, X. *Tian Jin Jian Chang Jian Zha Tu De Gong Cheng Li Yong Yan Jiu*; China Ocean Press: Beijing, China, 2013; pp. 1–5. (In Chinese)
4. Zhao, X.; Liu, C. Synthesis and Characterization of Fy ash Geopolymer Paste for Goaf Backfill: Reuse of Soda Residue. *J. Clean. Prod.* **2020**, *260*, 121045. [[CrossRef](#)]
5. Bellmann, F.; Stark, J. Activation of Blast Furnace Slag by a New Method. *Cem. Concr. Res.* **2009**, *39*, 644–650. [[CrossRef](#)]
6. Lothenbach, B.; Scrivener, K. Supplementary Cementitious Materials. *Cem. Concr. Res.* **2011**, *41*, 217–229. [[CrossRef](#)]
7. Junior, J.A.L.; Azevedo, A.R.G. Influence of Processing Parameters Variation on the Development of Geopolymeric Ceramic Blocks with Calcined Kaolinite Clay. *Case Stud. Constr. Mater.* **2022**, *12*, e00897. [[CrossRef](#)]
8. Bilginer, A.; Canbek, O. Activation of Blast Furnace Slag with Soda Production Waste. *J. Mater. Civ. Eng.* **2020**, *32*, 04019316. [[CrossRef](#)]
9. Yang, K.; Cho, A. Hydration Products and Strength Development of Calcium Hydroxide-based Alkali-Activated Slag Mortars. *Constr. Build. Mater.* **2012**, *29*, 410–419. [[CrossRef](#)]
10. Kim, M.S.; Jun, Y. Use of CaO as an Activator for Producing a Price-Competitive non-Cement Structural Binder Using Ground Granulated Blast Furnace Slag. *Cem. Concr. Res.* **2013**, *54*, 208–214. [[CrossRef](#)]
11. Burciaga-Díaz, O. Parameters Affecting the Properties and Microstructure of Quicklime (CaO)-Activated Slag Cement Pastes. *Cem. Concr. Compos.* **2019**, *103*, 104–111. [[CrossRef](#)]
12. Lin, Y.; Xu, D. Effect of Soda Residue Addition and Its Chemical Composition on Physical Properties and Hydration Products of Soda Residue-Activated Slag Cementitious Materials. *Materials* **2020**, *13*, 1789. [[CrossRef](#)]
13. Lin, Y.; Xu, D. Properties and Hydration Mechanism of Soda Residue-Activated Ground Granulated Blast Furnace Slag Cementitious Materials. *Materials* **2021**, *14*, 2883. [[CrossRef](#)]
14. Pan, Q. Discussion on Hydration Mechanism of Ground Granulated Blast Furnace Slag. *Cement* **2014**, *9*, 6–10. (In Chinese)

15. Ma, Y.; Liu, Z. Remediating Potentially Toxic Metal and Organic Co-Contamination of Soil by Combining in Situ Solidification/Stabilization and Chemical Oxidation: Efficacy, Mechanism, and Evaluation. *Int. J. Environ. Res. Public Health* **2018**, *15*, 2595. [[CrossRef](#)]
16. Song, S.; Jennings, H.M. Pore Solution Chemistry of Alkali-Activated Ground Granulated Blast Furnace Slag. *Cem. Concr. Res.* **1999**, *29*, 159–170. [[CrossRef](#)]
17. Kesim, A.G.; Tokyay, M. Properties of Alinite Cement Produced by Using Soda Sludge. *Adv. Cem. Res.* **2013**, *25*, 104–111. [[CrossRef](#)]
18. Gur, N.; Aktas, Y. Utilization of Soda Ash Plant Solid Wastes in Manufacture of Cement. *Elixir Cem. Concr. Compos.* **2012**, *47*, 8866–8873.
19. Uçal, G.O.; Mahyar, M. Hydration of Alinite Cement Produced from Soda Waste Sludge. *Constr. Build. Mater.* **2018**, *164*, 178–184. [[CrossRef](#)]
20. Potgieter, J.H.; Delpont, D.J. Chloride-Binding Effect of Blast Furnace Slag in Cement Pastes Containing Added Chlorides. *S. Afr. J. Chem.* **2011**, *63*, 108–114.
21. Runci, A.; Serdar, A. Effect of Curing Time on the Chloride Diffusion of Alkali-Activated Slag. *Case Stud. Constr. Mater.* **2022**, *16*, e00927. [[CrossRef](#)]
22. Li, H.; Farzadnia, N. The Role of Seawater in Interaction of Slag and Silica Fume with Cement in Low Water-to-Binder Ratio Pastes at the Early Age of Hydration. *Constr. Build. Mater.* **2018**, *185*, 508–518. [[CrossRef](#)]
23. Yuan, Q.; Shi, C. Chloride Binding of Cement-Based Materials Subjected to External Chloride Environment—A Review. *Constr. Build. Mater.* **2009**, *23*, 1–13. [[CrossRef](#)]
24. He, J.; Shi, X.K. Strength Properties of Dredged Soil at High Water Content Treated with Soda Residue, Carbide Slag, and Ground Granulated Blast Furnace Slag. *Constr. Build. Mater.* **2020**, *242*, 118126. [[CrossRef](#)]
25. He, J.; Wang, X. Shear Strength of Stabilized Clay Treated with Soda Residue and Ground Granulated Blast Furnace Slag. *J. Mater. Civ. Eng.* **2019**, *31*, 06018029. [[CrossRef](#)]
26. Song, R.; Zhao, Q. Microstructure and Composition of Hardened Paste of Soda Residue-Slag-Cement Binding Material System. *Front. Mater.* **2019**, *6*, 211. [[CrossRef](#)]
27. Xu, D.; Ni, W. Preparation of Clinker-Free Concrete by Using Soda Residue Composite Cementitious Material. *J. Harbin Inst. Technol.* **2020**, *52*, 151–160. (In Chinese)
28. Xu, D.; Ni, W. Ammonia-Soda Residue and Metallurgical Slags from Iron and Steel Industries as Cementitious Materials for Clinker-Free Concretes. *J. Clean. Prod.* **2021**, *307*, 127262. [[CrossRef](#)]
29. Sun, J.; Gu, X. Engineering Properties of the New Non-Nlinker Incorporating Soda Residue Solidified Soil. *J. Build. Mater.* **2014**, *17*, 1031–1035. (In Chinese)
30. Lin, Y.; Xu, D. Experimental Research on Mechanical Property and Microstructure of Blast Furnace Slag Cementitious Materials Activated by Soda Residue. *Bull. Chin. Ceram. Soc.* **2019**, *38*, 2876–2881. (In Chinese)
31. Wei, D.; Du, C. Preparation of a Composite Calcium Silicate Board with Carbide Slag and Coal-Based Solid Waste Activated by Different Alkali Activators. *ACS Omega* **2020**, *5*, 8934–8942. [[CrossRef](#)]
32. Huang, G.; Yuan, L. Cooperative Action and Compatibility Between Portland Cement and MSWI Bottom Ash Alkali-Activated Double Gel System Materials. *Constr. Build. Mater.* **2019**, *209*, 445–453. [[CrossRef](#)]
33. Scrivener, K.L.; Juilland, P. Advances in Understanding Hydration of Portland Cement. *Cem. Concr. Res.* **2015**, *78*, 38–56. [[CrossRef](#)]
34. Liu, Y.; Li, Y. Orthogonal Experiment on Performance of Mortar Made with Dune Sand. *Constr. Build. Mater.* **2020**, *264*, 120254. [[CrossRef](#)]
35. Wang, Y.; Qiu, J. Factors Affecting Brittleness Behavior of Coal-Gangue Ceramsite Lightweight Aggregate Concrete. *Front. Mater.* **2020**, *7*, 554718. [[CrossRef](#)]
36. Ye, J.; Zhang, W. Setting Acceleration and Strength Enhancement Derived from Calcium Species for Alkali-activated Cementitious Materials. *J. Chin. Ceram. Soc.* **2017**, *45*, 1101–1112. (In Chinese)
37. Temuujin, J.; Van Riessen, A. Influence of Calcium Compounds on the Mechanical Properties of Fly Ash Geopolymer Pastes. *J. Hazard. Mater.* **2009**, *167*, 82–88. [[CrossRef](#)]
38. Qu, X.; Zhao, Z. Heat Release Characteristics of Lime and Time-Dependent Rheological Behaviors of Lime-Activated Fly Ash Pastes. *Case Stud. Constr. Mater.* **2022**, *16*, e01043. [[CrossRef](#)]
39. Zhang, L.; Song, S. Effect of Gypsum Content on Properties of Alkali-Activated Slag Cement Mortar. *Appl. Chem. Ind.* **2020**, *49*, 2168–2172+2177. (In Chinese)
40. Yum, W.S.; Jeong, Y. Effects of CaCl<sub>2</sub> on Hydration and Properties of Lime (CaO)-Activated Slag/Fly Ash Binder. *Cem. Concr. Compos.* **2017**, *84*, 111–123. [[CrossRef](#)]
41. GB/T 17671-1999; Method of Testing Cements—Determination of Strength. General Administration of Quality Supervision, Inspection and Quarantine of the People’s Republic of China: Beijing, China, 1999. (In Chinese)
42. Zhao, X.; Wang, H. Resistance of Soda Residue–Fly Ash Based Geopolymer Mortar to Acid and Sulfate Environments. *Materials* **2021**, *14*, 785. [[CrossRef](#)]
43. GB/T 2419-2005; Test Method for Fluidity of Cement Mortar. General Administration of Quality Supervision, Inspection and Quarantine of the People’s Republic of China: Beijing, China, 2005. (In Chinese)

44. ASTM C20-2000(2005); ASTM International. Standard Test Methods for Apparent Porosity, Water Absorption, Apparent Specific Gravity, and Bulk Density of Burned Refractory Brick and Shapes by Boiling Water. ASTM International: West Conshohocken, PA, USA, 2010.
45. GB 175-2007; Common Portland Cement. General Administration of Quality Supervision, Inspection and Quarantine of the People's Republic of China: Beijing, China, 2007. (In Chinese)
46. Huang, G.; Ji, Y. Improving Strength of Calcinated Coal Gangue Geopolymer Mortars via Increasing Calcium Content. *Constr. Build. Mater.* **2018**, *166*, 760–768. [[CrossRef](#)]
47. Qiao, C.; Suraneni, P. Chloride binding of cement pastes with fly ash exposed to CaCl<sub>2</sub> solutions at 5 and 23 °C. *Cem. Concr. Compos.* **2019**, *97*, 43–53. [[CrossRef](#)]
48. Ipavec, A.; Vuk, T. Chloride Binding into Hydrated Blended Cements: The Influence of Limestone and Alkalinity. *Cem. Concr. Res.* **2013**, *48*, 74–85. [[CrossRef](#)]
49. Zhu, Q.; Jiang, L. Effect of Chloride Salt Type on Chloride Binding Behavior of Concrete. *Constr. Build. Mater.* **2012**, *37*, 512–517. [[CrossRef](#)]